doi:10.36487/ACG_repo/2063_36

Back analysis of cave propagation and subsidence at Cadia East Mine

E Ghazvinian Itasca Consulting Group, United States

M Fuenzalida Itasca Consulting Group, United States

C Orrego Newcrest Mining Limited, Australia

M Pierce Pierce Engineering, United States

Abstract

Cadia East panel cave mine is one of the three mines comprising the Cadia Valley Operations, one of Australia's largest gold mining operations, located in New South Wales. Production at Cadia East commenced in 2013 from Panel Cave 1 (PC1) with its extraction level set at a depth of 1,200 m below the surface. Currently, ore is extracted from PC1 and its neighboring panel (PC2) with an extraction level at 1,400 m depth. A critical component of effective production for Cadia East is successful cave propagation to the surface considering significant cave heights. To ensure cave performance, the rock mass immediately above the footprint of PC1 and PC2 was pre-conditioned by means of hydraulic fracturing (combined with blasting for PC1). Furthermore, a surface hydraulic fracturing program had to be instigated in the hard and competent near surface rock mass above PC1 to assist cave propagation through the final 450 m and its breakthrough to the surface. This paper discusses the significance of using a strain-softening model with the ability to capture the correct mechanics of rock mass frictional strength mobilization for a precise back-analysis of cave performance. IMASS (Itasca Model for Advanced Strain Softening) was used for this study in FLAC3D. IMASS uses two-mode softening yield surfaces. The first residual envelope represents the post-peak strength, and the second residual envelope represents the ultimate rock mass residual strength. The two-mode softening allows for mobilization of high apparent friction angles at low confinement when the blocks are formed in the rock mass. This, in combination with implementation of pre- and post-conditioning of the rock mass (hydraulic fracturing program) in the simulation, were critical in the successful calibration of the model.

1 Introduction

The success of the Ridgeway sublevel cave at Cadia Valley Operations (CVO) has led to expansion of block caving operations, initially at Ridgeway Deeps (RWD) and more recently at Cadia East panel cave mine. Cadia is one of Australia's largest gold mining operations, located in New South Wales, is characterized by high-stress, hard rock mining conditions. The combination of a deep, high-stress environment, a competent rock mass and the ability to use very high lifts at depths between 1,200 and 1,400 m provides a unique opportunity for Cadia East to maximize return. Establishment of Panel Cave 1 (PC1) at Cadia East commenced in early 2011 with its extraction level set at a depth of 1,200 m below the surface. Official production from PC1 began in 2013. Currently ore is extracted from PC1 and its neighboring panel (PC2) with an extraction level at 1,400 m depth (Figure 1). Figure 2 shows the significance of achieving two propagating cave columns in Cadia East to surface from depths of up to 1400 m in a single lift when compared to other established block and panel caving operations (Cuello & Newcombe 2018). Rock mass preconditioning was a key component of cave establishment at Cadia East to assist caveability, ensure the successful propagation of the cave to the surface (Manca & Flores 2013) and manage mine induced seismicity (Lowther et al. 2016.)

Newcrest plans to further develop panel caves for the Cadia East deposit, as extensions to the current PC1 and PC2 operations, over the coming decades. Figure 1 shows the preliminary plan for the extension of the Western and Eastern caves. This instigated a back-analysis of PC1 and PC2 propagation and subsidence

and the associated rock mass damage around the crater to optimise the accuracy of geomechanical design parameters. The resulting calibrated model will provide a means to conduct a predictive analysis using the planned production in order to estimate further subsidence and the likelihood of damage to critical surface and underground infrastructure.

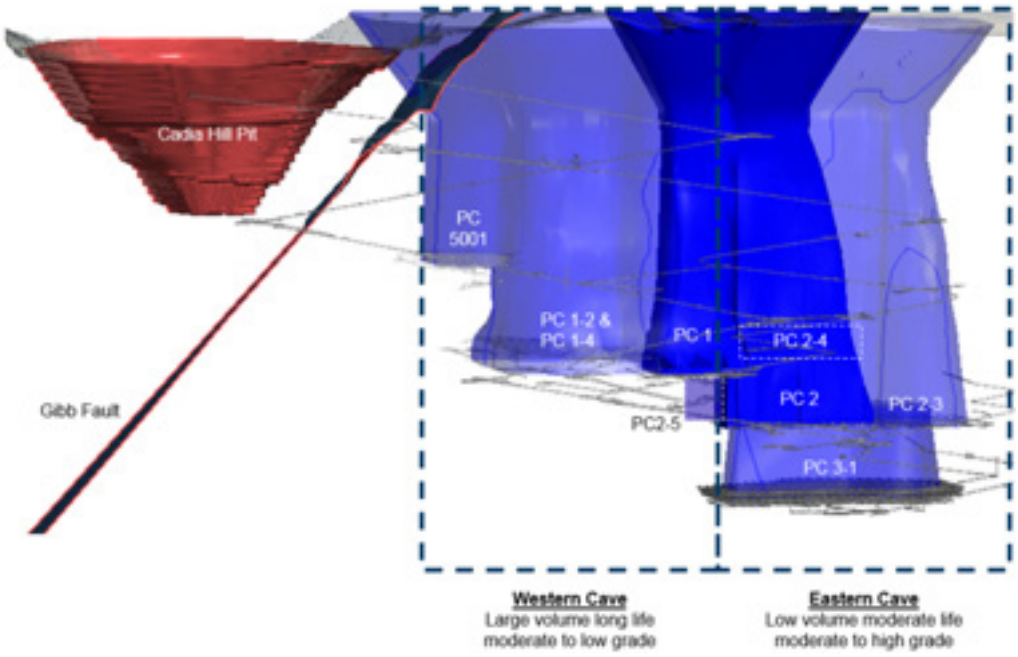

Figure 1 Location of PC1 and PC2 panel caves (Newcrest 2018)

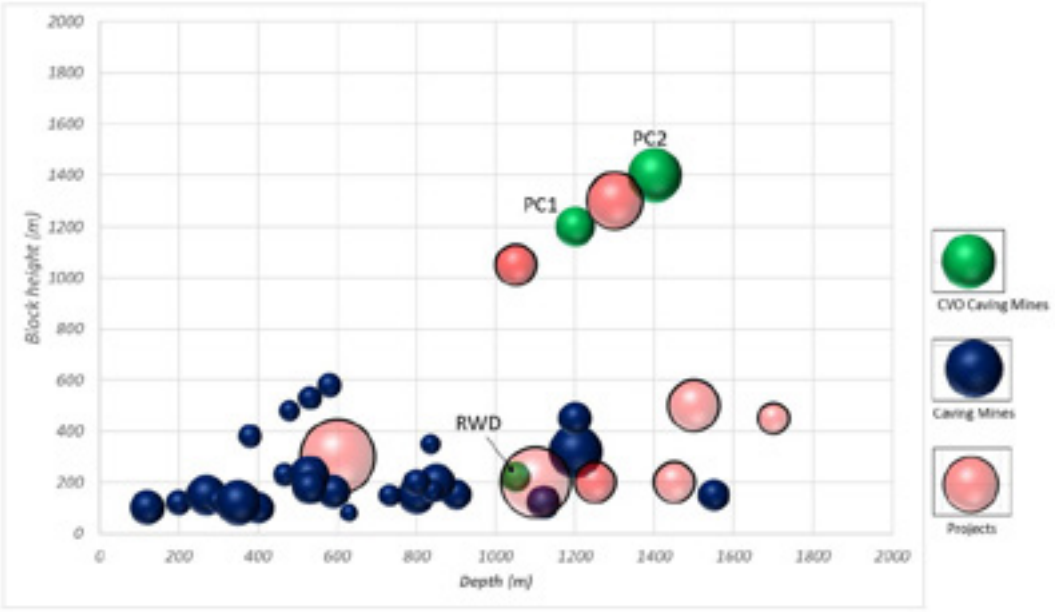

Figure 2 The relationship between depth, block height and maximum production footprint (bubble size) for caving operations (Cuello & Newcombe 2018)

2 Modeling approach

A large-scale FLAC3D (Itasca 2019) model was constructed to simulate the regional extent of the Cadia Valley Operations. It included the Cadia Hill open pit to capture the correct pre-mining in-situ stress condition (prior to cave mining) as listed in Table 1. The four lithologies with major impacts on the cave growth that were represented in the model are shown in Figure 3 for an east-west cross-section through the extraction panel. Geological structures such as faults and shear zones were not included in the current, first pass assessment of the PC2-3 LoM subsidence. Production was simulated from Panels PC1, PC2, PC2-3 and PC1-2 from fiscal year 2012 to fiscal year 2035 (Figure 3) using the "caving algorithm".

In 2019, production was performed from Panels PC1 and PC2 with plans for future production, in order, from extraction panels PC2-3 and PC1-2.

The caving model in this study is benefitting from Itasca's latest strain-softening constitutive model, IMASS (Itasca Model for Advanced Strain Softening). IMASS uses a two-stage softening behavior. The mechanical and mathematical background for IMASS is described in Section 2.2. Furthermore, implementation of pre- and post-conditioning of the rock mass (hydraulic fracturing program) played an important role in the simulation. This is discussed in detail in Section 3.1.

Table 1 In-situ stress tensor used in this study (Lee 2012)

Principal stress	Regime magnitude criteria (MPa), depth in (m)	Dip	Bearing
σ1	5.0 + (0.0479 x depth)	00 deg	074 deg
σ2	0.0 + (0.0344 x depth)	00 deg	164 deg
σ3	0.0 + (0.0297 x depth)	90 deg	074 deg

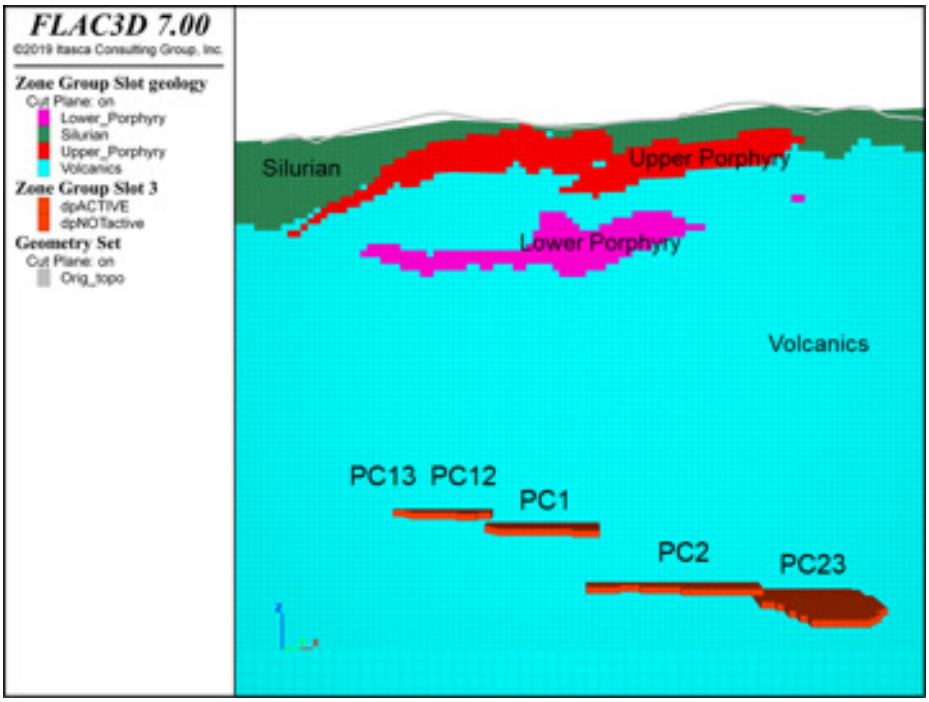

Figure 3 East-west cross-section showing the lithologies represented in the model

2.1 Caving algorithm

A numerical approach to cave assessment has been developed by Itasca (Board & Pierce 2009; Sainsbury 2012) over the past 15 years during the industry-funded International Caving Study (ICS I & II) and Mass Mining Technology (MMT) projects. The approach considers the changes that the rock mass experiences when caving occurs (cohesion and tension weakening, post-peak brittleness, modulus softening and dilation) and correctly represents production as it progresses in time.

To simulate draw, a layer of zones encompassing all active drawpoints for the current year are deleted within the model. Forces are applied to gridpoints on the floor of the deleted volume to represent the resistance provided by the extraction level, while the gridpoints on the roof of the deleted volume have a small downward velocity applied to them that is proportional to the relative draw rate for the nearest drawpoint. The largest pull velocity (i.e., for the drawpoints with the highest production rate) is set low enough to ensure pseudo-static equilibrium throughout the model (i.e., to allow natural gravitational flow of the material and to avoid dynamic 'pulling' of the overlying material). The model

is run in small-strain mode (i.e., gridpoint coordinates are not updated); thus, the density of the zones within the cave must be updated constantly (based on the emergent volumetric strain) to maintain mass balance (Figure 4).

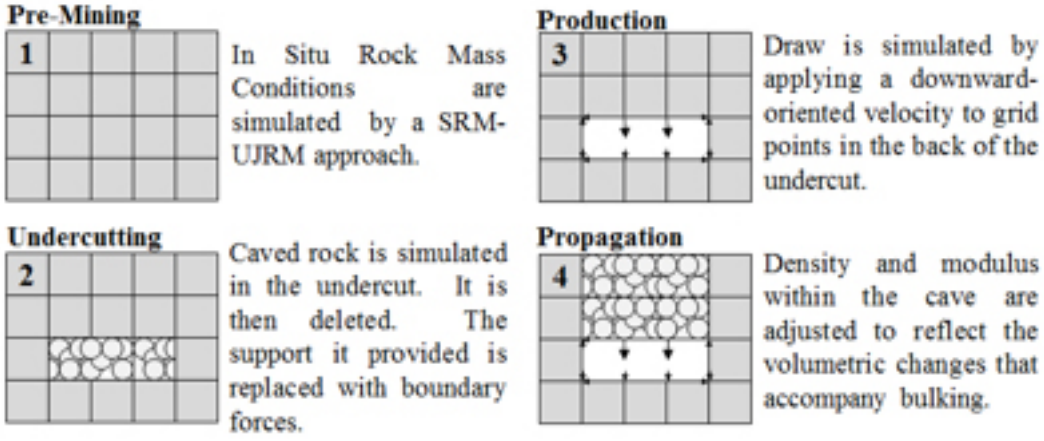

Figure 4 Simulation of production draw from FLAC3D model based on velocities (Sainsbury et al. 2011)

By summing the masses drawn by all the nodes (gridpoints), the total production from the cave within the model may be calculated at any point in time. The model is cycled until the mass produced from the numerical cave is consistent with what is to be produced from the actual cave for the current time increment (as defined by the draw schedule). As the mass is drawn from the model, displacement and yielding can occur in the overlying zones (dictated by the stress state and yield strength of the rock mass) and the cave may progress upward. The process is repeated for the remaining years in the schedule. As old drawpoints cease production, the surrounding zones are converted to a cohesionless caved rock material with a modulus consistent with a bulking factor of 40%, based on Pappas and Mark's work (Pappas & Mark 1993). This allows stresses to redistribute back into exhausted areas of the cave. This algorithm (referred to as "the caving algorithm") is used to simulate cave growth successfully at many mines around the world

A compatible constitutive model must go hand in hand with the caving algorithm. A constitutive model that represents the caving process must account for the progressive failure and disintegration of the rock mass from an intact/jointed to a caved material. In this complex process, creation of the cave results in: 1) deformation and stress redistribution of the rock mass above the undercut; 2) failure of the rock mass in advance of the cave, with associated progressive reduction in strength from peak to residual levels; and 3) dilation, bulking, fragmentation, and mobilization of the caved material. The failure process is characterized by shearing along pre-existing joint surfaces and stress-induced fracturing of intact rock blocks. The failure process will require shear or tensile failure of intact rock bridges between joint segments as the rock mass fragments. This overall process—loading of the rock mass to its peak strength, followed by a post-peak reduction in strength to some residual level with increasing strain—often is termed a "strain-softening" process and is the result of strain-dependent material properties.

2.2 Itasca model for advanced strain softening (IMASS)

The caving algorithm makes use of the Itasca Model for Advanced Strain Softening (*IMASS*) constitutive model in *FLAC3D*, which allows for representation of modulus softening, density adjustment, dilation, dilation shutoff, scaling of properties to zone size, cohesion weakening, tension weakening, and frictional strengthening. IMASS is Itasca's most advanced strain-softening model for simulation of rock mass response to mining. This model contains two softening yield surfaces as shown in Figure 5. The Hoek-Brown (H-B) parameters of the residual strength envelopes are selected to approximate the peak shear strength for rockfill material as defined by Barton & Kjaernsli (1981):

$$\tau = \sigma_n \tan\left(R.\log\left(\frac{S}{\sigma_n}\right) + \emptyset_b\right) \quad (1)$$

where τ is shear strength, σ_n is the normal stress, *R* is equivalent roughness (Figure 6), *S* is the rock block strength, and ϕ_b is the basic friction angle for the rock.

The first residual envelope represents the post-peak strength. At this point, the rock mass is assumed to have undergone fracturing, but the resulting rock fragments are still fully interlocked. Consequently, porosity is considered to be close to zero. The second residual envelope represents the ultimate rock mass residual strength at the point of maximum bulking. At this point, the degree of rock fragment interlock is at its minimum, and the porosity is maximized (maximum porosity of 40% is assumed). Ideally, the first and second residual envelopes describe the behavior of cohesionless, perfectly frictional material with different degrees of interlocking. The Hoek-Brown approximation of Equation 1 that is implemented in IMASS assumes formation and interaction of very sharp, angular and very rough fragments during the course of bulking, from porosity 0% to 40% on Barton & Kjaernsli (1981) nomogram (Figure 6).

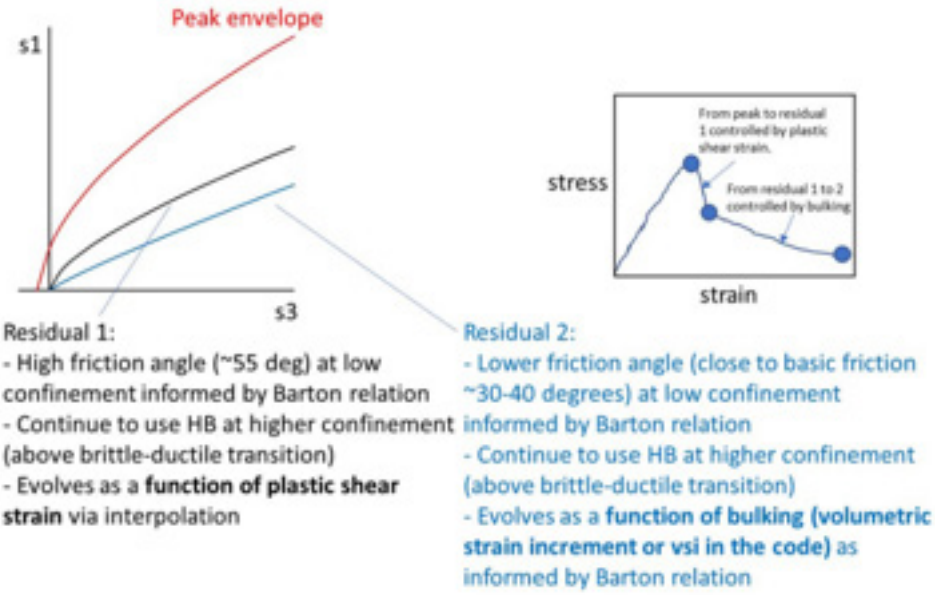

Figure 5 Yield surfaces and material response for IMASS model

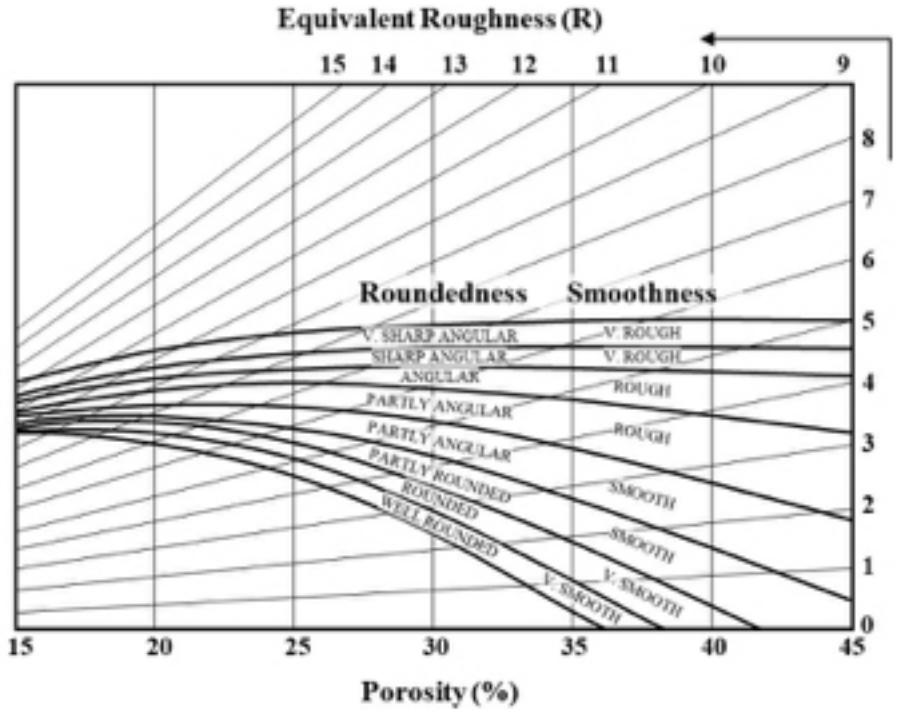

Figure 6 Equivalent roughness of an assembly of rock fragments based on porosity and fragment roundedness/ smoothness (Barton & Kjaernsli 1981)

3 Back analysis of historical subsidence

Measured ground surface depression was the most accurate information that was available and could be tied to the cave propagation for the Cadia East mine. The goal of the calibration process was to match, as closely as possible, the fracture limit observed at the mine for Financial Year 2017 (FY17), FY18, and FY19 with the model predictions. Among others, the following items were the key components investigated within the calibration effort:

- Implementation of pre- and post-conditioning by using ubiquitous joints (UBI) in the model.
  - Examining the effect of UBI orientation on model response (installed horizontal or perpendicular to minor principal stress).
  - Investigating the effect of friction and dilation angles along the UBIs on model response.
  - Implementing a routine to inject stresses within the pre- and post-conditioned zones to capture rock mass bulking due to residual aperture in hydraulic fracture (HF) planes.
- Implementing a buckling scheme to capture deconfinement and stress relaxation for beams generated by hydraulic fracturing.
  - Fine-tuning the stress thresholds used in the buckling scheme.
- Assessing the effect of rock mass dilation angle.
- Investigating different bulking potentials for the rock mass and within the pre- and post-conditioned volumes.

The peak rock mass properties for the lithologies represented in the model and the calibrated properties discussed in this section are listed in Tables 2 and 3, respectively.

Table 2 Rock mass properties used for the analysis

Lithology	Density (kg/m³)	GSI	Intact rock strength (MPa)	H-B mi	Intact Young's Modulus (GPa)	Dilation angle (°)
Volcanics	2,800	47	156	18	40	10
Silurian	2,690	30	50	12	25	10
Lower Porphyry	2,780	49	168	25	45	10
Upper Porphyry	2,780	43	80	20	30	10

Table 3 Calibrated properties used for the analysis

Lithology	IMASS residual 1			IMASS residual 2			Max. Bulking	UBI Friction Angle (residual)	UBI Dilation Angle (residual)
	H-B m	H-B a	H-B s	H-B m	H-B a	H-B s			
All lithologies without pre- or post-conditioning	2.0	0.6	0	2.0	0.85	0	0.4	-	-
All lithologies with pre- or post-conditioning	2.0	0.6	0	2.0	0.85	0	0.05	30 (30)	3 (3)

3.1 Hydraulic fracturing program at Cadia East

Assisting caveability is becoming important as a growing number of mining companies are establishing large-scale cave mines in hard, competent rock masses. A number of these new cave mines are being established at considerable depths (greater than 1,000 m) with high cave column heights. Cave mining was not perceived to be suitable for those conditions previous to the application of preconditioning (hydraulic fracturing and confined blasting) to assist the rock mass breaking in caving. At Cadia East, where extraction levels exceed 1,000 m in depth, underground-based hydraulic fracturing is routinely performed as a means of preconditioning the orebody to reduce the magnitude of large seismic events occurring within and outside the footprint during cave establishment, propagation and breakthrough phases and to assist in cave propagation and fragmentation (Lowther et al. 2016; Flores-Gonzalez 2019; Pardo & Rojas 2016).

Preconditioning of the rock mass above the PC1 extraction level ensured self-propagation of the cave when it reached its critical hydraulic radius. The cave propagated continuously with an average caving rate between 3.0 and 4.5 m/day until it propagated past 750 m in height approaching the competent Lower Capping Porphyry (see Figure 3). The combination of this overlying competent geological layer and loss of driving stress with decreasing depth promoted the narrowing of the cave crown and reducing the caving rate. This invoked a surface-based hydraulic fracturing program to stimulate the cave to propagate through the final 450 m to surface. The surface hydraulic fracturing program was successfully implemented through three boreholes. A total of 245 fractures were completed by 11th September 2014 and cave breakthrough occurred on 22nd October 2014 with the caving rate reaching approximately 65 m/day (Lowther et al. 2016).

3.1.1 Simulation of hydraulic fracturing treatment

Pre- and post-conditioning of the rock mass in the model was simulated by means of ubiquitous joints (UBIs). They were installed perpendicular to the orientation of minor principal stress at the time of treatment. A cohesionless, perfectly plastic behavior in terms of friction and dilation angle was assumed for the UBIs. A peak and residual friction angle of 30° as well as peak and residual dilation angle of 3° were the calibrated values. Figure 7 shows the HF-treated parts of the rock mass. Those volumes assume a radius of 60 m for the hydraulic fractures. The bulking limit for the rock mass in those parts was limited to 0.05 while the rest of the rock mass was allowed to bulk up to a factor of 0.4. In IMASS, the dilation angle will drop to zero and density adjustment due to bulking will shut off when the volumetric strain increment for a zone reaches the prescribed bulking limit.

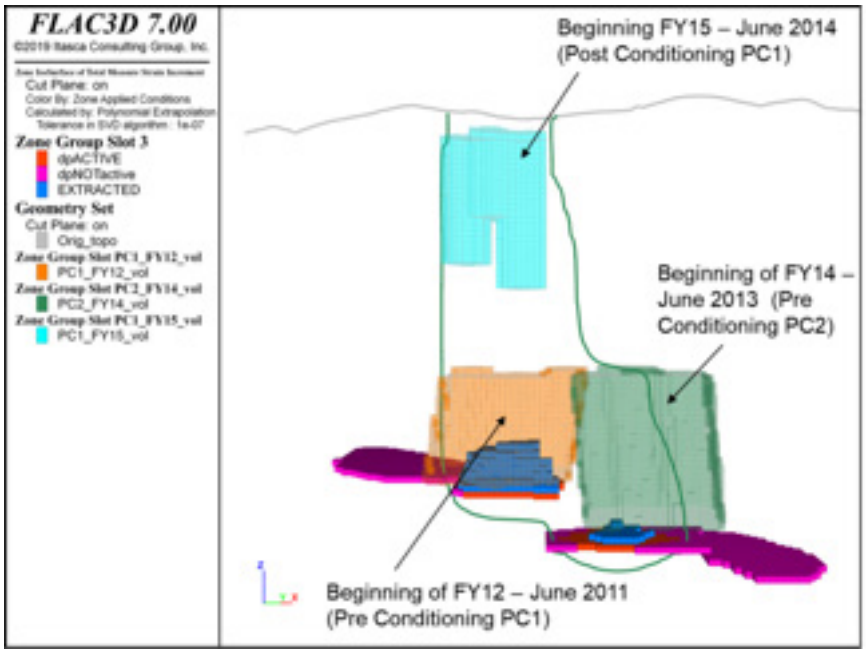

Figure 7 Implementation of pre- and post-conditioning of the rock mass in the model by using ubiquitous joints

3.1.2 *Buckling scheme*

A buckling scheme was implemented in the model to capture deconfinement and stress relaxation for beams generated by hydraulic fracturing (Bouzeran et al. 2019). The continuum model in this study cannot directly capture the mechanics involved in the buckling process because of the absence of joint interfaces in the model to represent the HF planes. The buckling scheme uses the two input parameters *Sig(normal)* and *Stress_ratio* to find target zones in the following steps:

- Stress is calculated normal to the UBI plane and compared with *Sig(normal)*.
- The maximum in-plane stress for UBIs is calculated and compared with target Sig(in-plane) = (UBI normal stress) × *Stress_ratio*.

For a zone, if (UBI normal stress < Sig(normal)) and (UBI in-plane stress > Sig(in-plane)), then stresses in that zone are zeroed and residual properties (R1) are applied. From the calibration process, it was determined that *Sig(normal)* = 4.0 MPa and *Stress_ratio* = 5.0.

3.2 Estimation of fracture limit

In this study, the extent of fracture limit is defined by an isosurface of the total measure of strain with a value of 5E-3 (Cavieres et al. 2003). The total measure of strain is defined as $\varepsilon_{tm} = \sqrt{\varepsilon_1^2 + \varepsilon_2^2 + \varepsilon_3^2}$ where ε_1, ε_2 and ε_3 are the major, intermediate and minor principal strains, respectively. This limit delineates the extents of visible fracturing that would be expected from orebody extraction.

The agreement between the fracture limits predicted by the model and field observations are shown in Figure 8, Figure 9, and Figure 10 for FY17, FY18, and FY19, respectively. The figures indicate that the calibrated model predicts the fracture limit with a good proximity to field observations. In addition, the model successfully captures the abrupt expansion of fracture limit between FY17 and FY18. The implementation of the buckling scheme was instrumental in capturing the plug movement above the PC1 panel (Figure 11), which made proper conditions for accurate prediction of the fracture limit for FY17 to FY19.

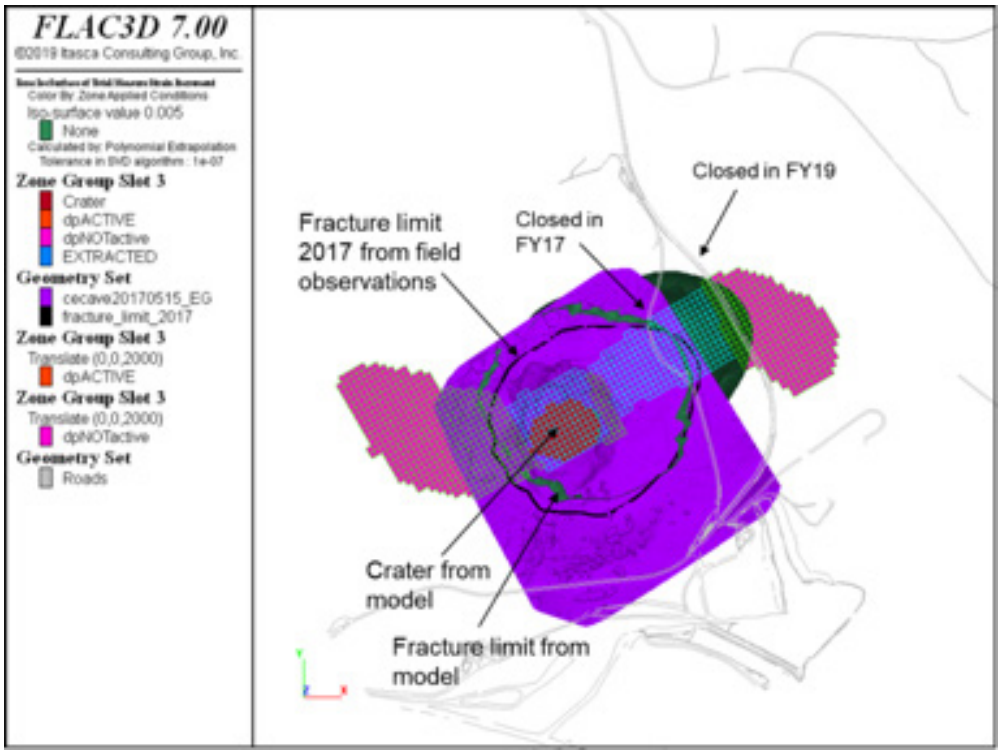

Figure 8 Comparison between the field observation and model predicted fracture limits for FY17

The simulated overhang between the PC1 and PC2 caves, identified with the blue dashed line in Figure 11, is another essential component of this calibration. The two-mode softening yield surfaces allows for mobilization of a high apparent friction angle at low confinement (when blocks are formed in the rock mass due to fracturing). This mobilized post-peak strength is playing a key role on the stability of the observed overhang. With further production from PC2 and the associated bulking, the rock mass quality diminished into its ultimate residual strength with lower friction angle. At this point, the interaction between the PC1 cave and PC2 cave moves the overhang to a higher elevation.

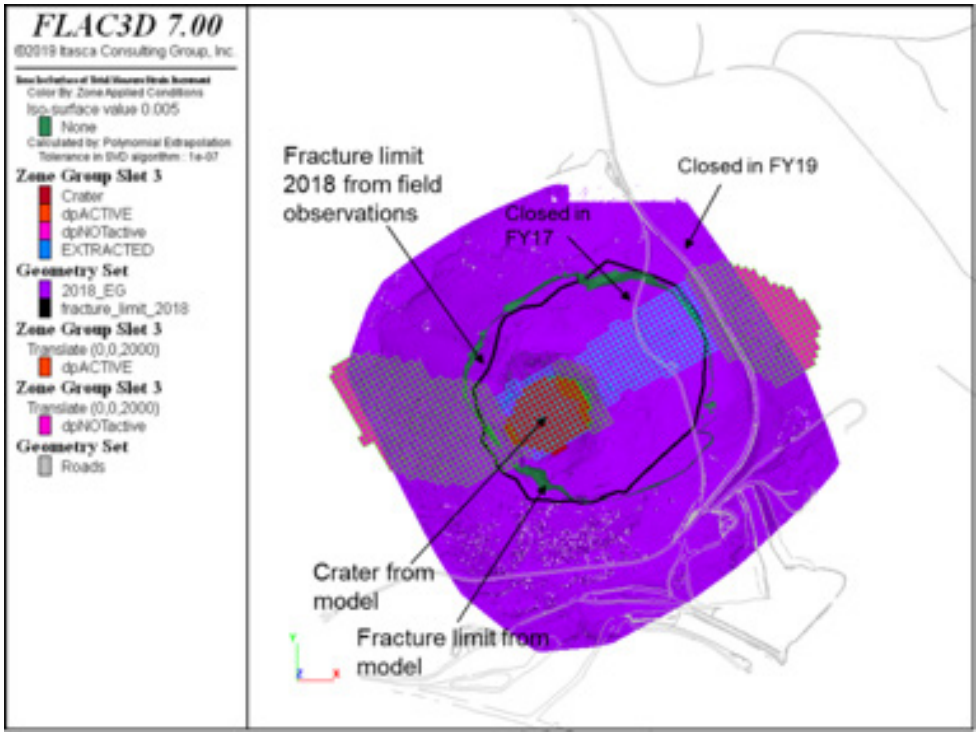

Figure 9 Comparison between the field observation and model predicted fracture limits for FY18

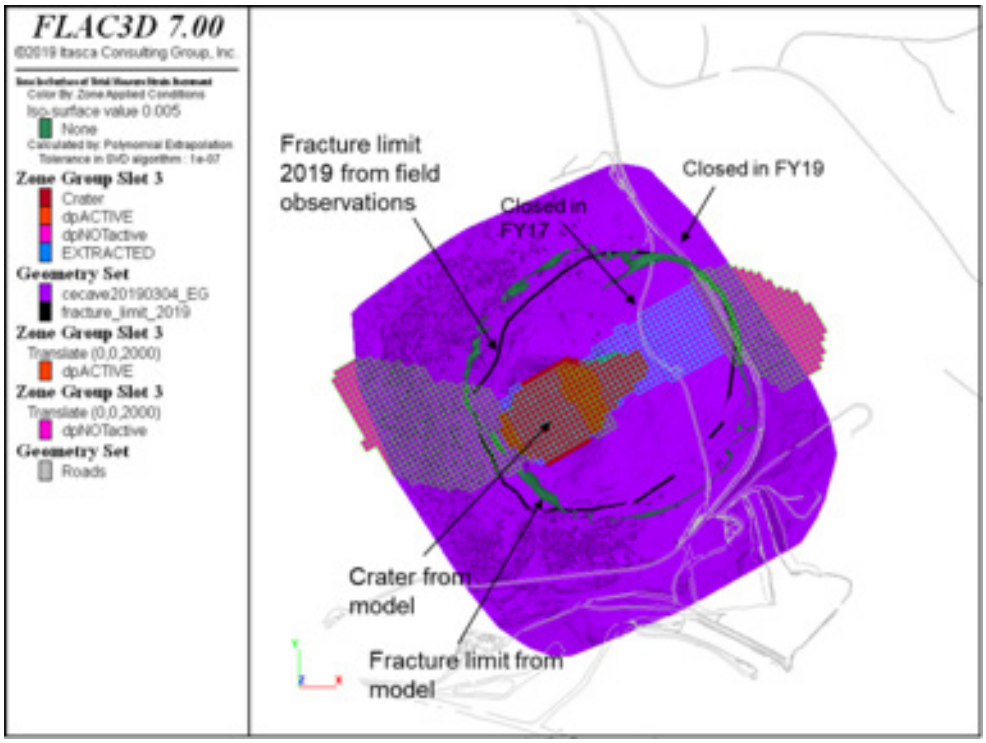

Figure 10 Comparison between the field observation and model predicted fracture limits for FY19

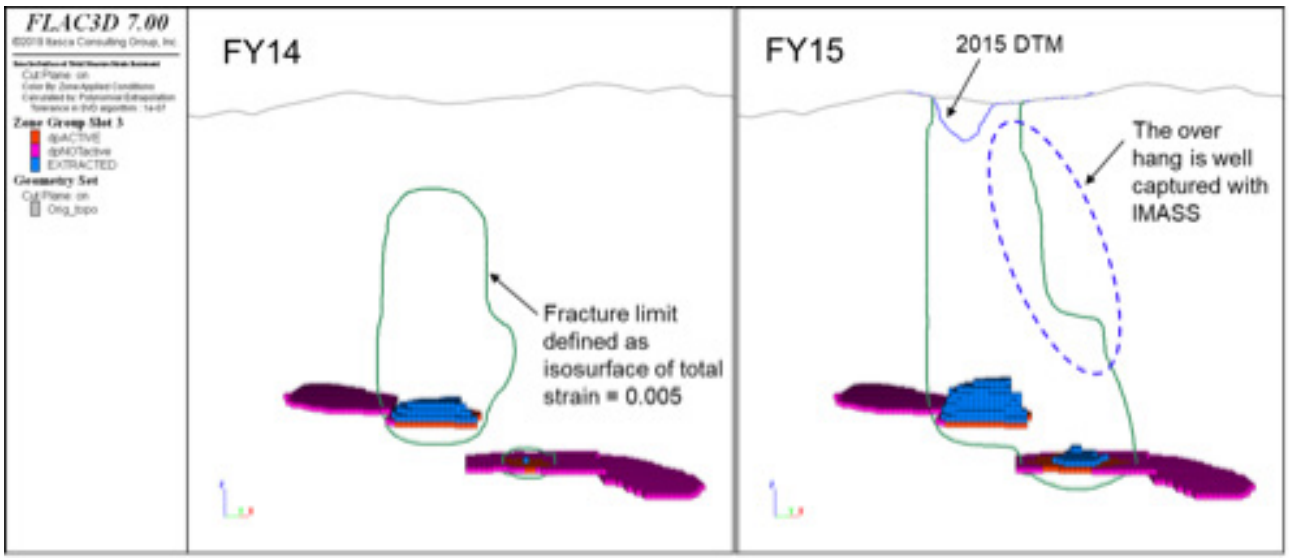

Figure 11 Fracture limits before and after implementation of surface-based hydraulic fractures

3.3 Delineation of surface damage

The surface subsidence outside the fracture limit is characterized in this study by a combination of horizontal strain and angular distortion. Different combinations of those two parameters define damage categories for surface infrastructure as shown in Figure 12. A qualitative description of each damage category is given in Harrison (2011). It should be noted that the surface damage categories in Harrison (2011) are developed based on observations of building damages and should be used with caution if applied to other types of infrastructure. In general, those damage limits are subjective to the standards followed by each mine, as their tolerances to subsidence differ.

It is shown in Figure 13 and Figure 14 that category 5 damage intersects with the access road and the replacement access road in FY17 and FY19, respectively. This closely replicates the observations at the site, whereby the initial access road was closed in March 2017 (FY17) and the replacement access road was taken out of service in November 2018 (FY19) due to surface cracking. This suggests that a good correlation can be established between the damage limits and serviceability of the surface infrastructure depending on the mine's tolerance for risk.

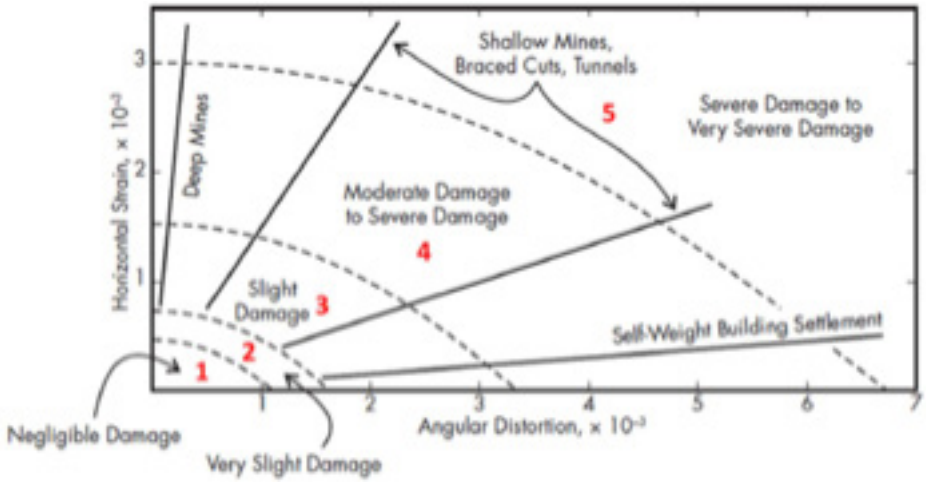

Figure 12 Different categories of building damage as determined from a combination of horizontal strain and angular distortion (after Harrison 2011)

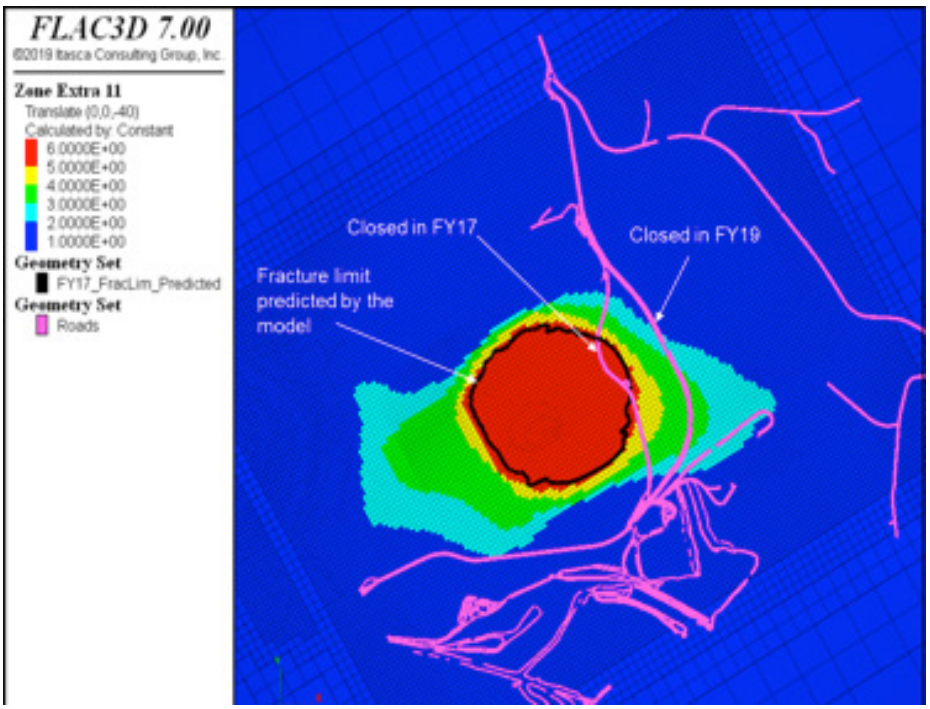

Figure 13 **Smoothed contour of surface damage categories based on Harrison (2011) — FY17 (smoothing sphere radius = 80 m)**

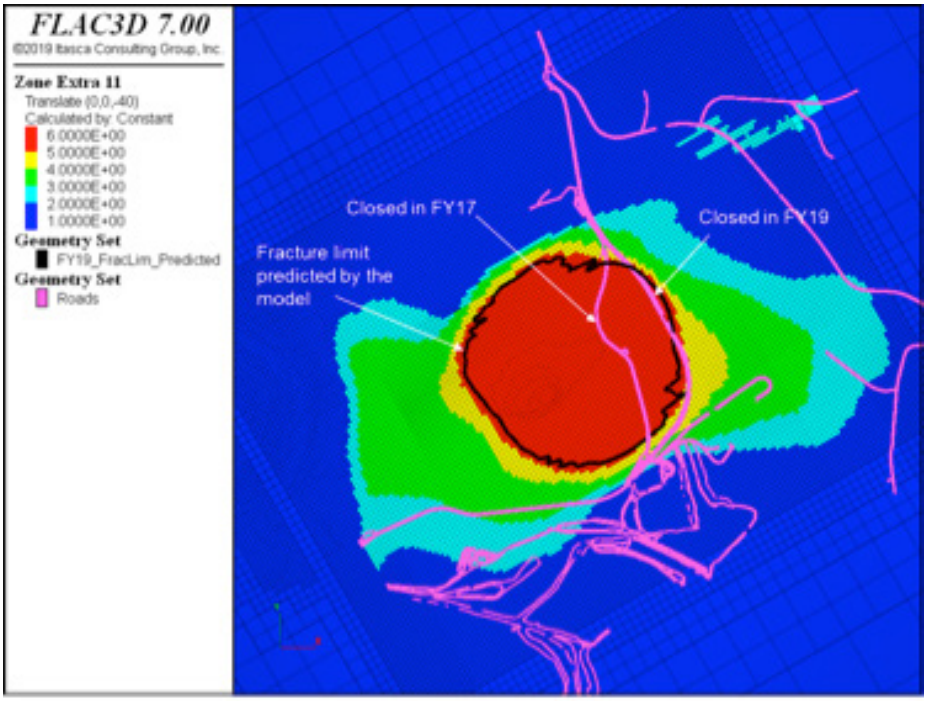

Figure 14 **Smoothed contour of surface damage categories based on Harrison (2011) — FY19 (smoothing sphere radius = 80 m)**

4 PC2-3 LoM subsidence analysis and forecasting of serviceability limit for critical infrastructure

The main purpose of this study was to identify the potential surface subsidence for the planned production scenario over the PC2-3 LoM (FY35) as well as the serviceability assessment of critical surface and underground infrastructure. Different paths were taken to analyze the stability of surface versus underground infrastructure. This section provides a general overview of those approaches.

4.1 Serviceability limit for surface infrastructure

The serviceability limit for critical surface infrastructure such as public roads, a warehouse, and vent raises were analyzed using a combination of surface damage categories (Figure 15) and the predicted total strain (Figure 16). The tolerance of different structures to subsidence is different, which should be considered in the analysis. For instance, vent raises with mechanical equipment (e.g., fans) on the surface have stricter tolerance to subsidence compared to other vent raises intersecting the ground surface. It should also be noted that the vent raises were assessed under both surface and underground serviceability limit studies for their segments near the surface and at depth, respectively.

4.2 Serviceability limit for underground infrastructure

The underground vent raises and drives were not explicitly simulated in the numerical model for computational efficiency. However, the discretization surrounding the critical infrastructure was refined to capture accurate stress evolution as well as induced strains. To examine serviceability of critical vent raises and drives over the planned PC2-3 LoM, the following were painted over their wireframes:

1. Stress to strength ratio: Estimated stress concentration in the walls of underground openings were compared to the spalling strength of the rock at near-zero confinement to provide an estimate of stress damage potential.

2. *Sloss* (a damage indicator in the IMASS constitutive model)

   Sloss changes between [1,-1]:

   Between Peak and first residual envelope:

   Sloss = 1 – (plastic shear strain/critical plastic shear strain)

   Between first and second residual envelope:

   Sloss = – (volumetric strain/maximum allowable volumetric strain)

Figure 17 schematically represents *Sloss* for different degrees of damage in a rock mass. At "C" the rock mass is assumed to have undergone fracturing, but the resulting rock fragments are still fully interlocked (cohesion in the rock mass is completely lost but friction is high). At this point the stress is above the spalling or fracturing strength of the rock. However, experience has shown that the underground opening is stable with minimal support. At "D" the degree of rock fragments interlocking is at its minimum and the porosity is maximized. Unlined vent raises or minimally supported drives at this stress state are considered unserviceable.

Comparison of field observation and numerical results for the access drift to the 5050 Engineering Level indicated that partial or complete loss of cohesion in the rock mass (i.e., stress to strength ratio > 1.0) does not necessarily translate to major damages to the underground openings, since a high degree of interlock and cohesion is still maintained (as long as they are supported, except maybe vertical vent raises that could remain stable unsupported with all cohesion lost). Therefore, the calibrated Sloss of -0.1 (based on field observations) was used as the threshold to determine the serviceability limit for the drives in the predictive modeling. This is consistent with the earlier discussion in this paper that bulking of the rock mass is the main controlling factor for serviceability of the underground infrastructure (in comparison to cohesion loss).

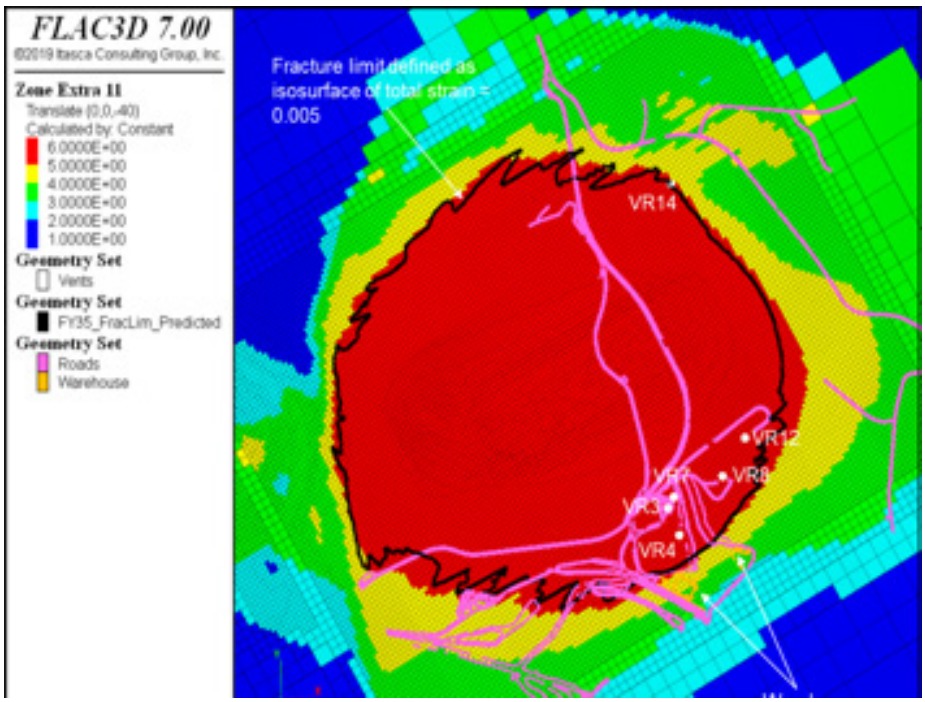

Figure 15 Smoothed contour of surface damage categories based on Harrison (2011) — FY35 (smoothing sphere radius = 80 m)

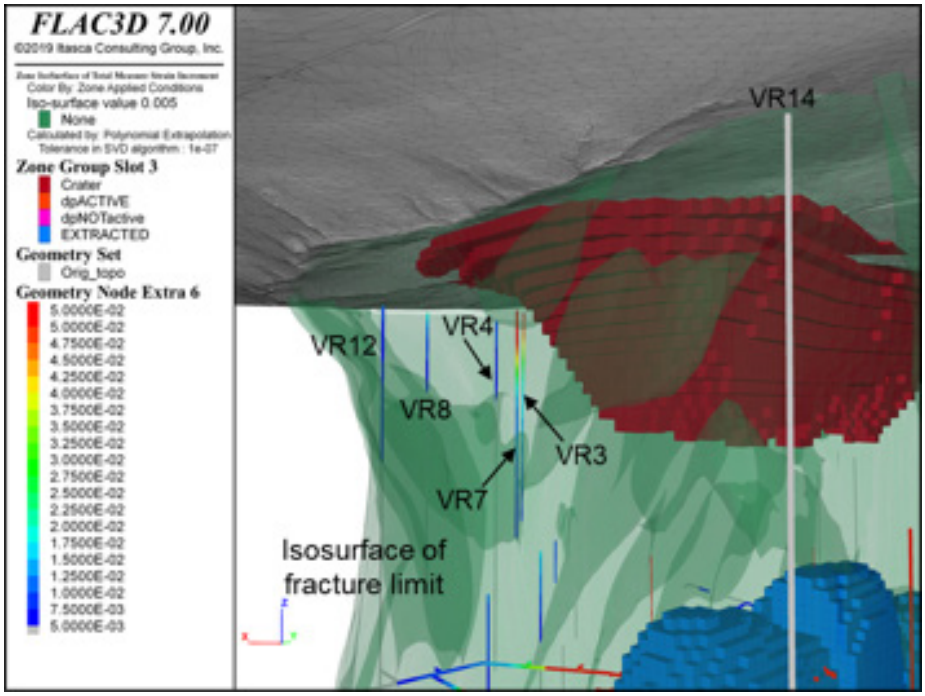

Figure 16 Contour of total strain painted over vent raises near the ground surface for FY35

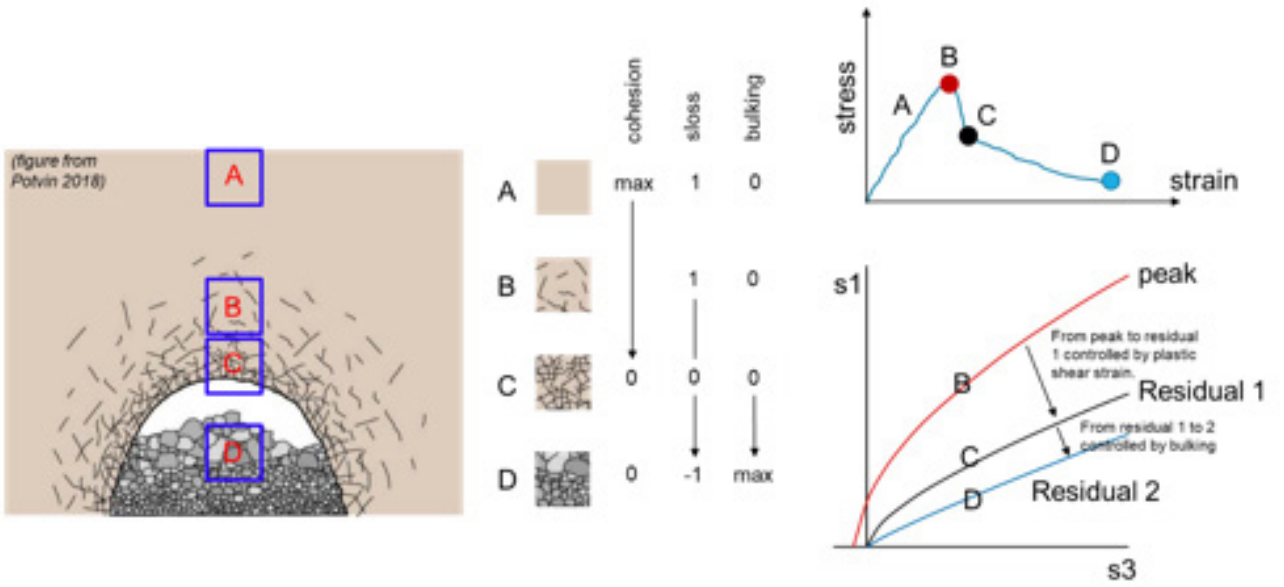

Figure 17 Schematic representation of Sloss for various degrees of damage in a rock mass

An example for serviceability assessment of the 5050 Level perimeter drive at the end of production is shown in Figure 18. Sloss is painted over the infrastructure wireframe on the left and stress to strength ratio is shown on the right. Black wireframes on the right denote parts of the drives where the stresses are greater than the fracturing strength of the rock (cohesion is completely or partially lost), meaning parts of the perimeter drive can experience damage in the form of shotcrete cracking or other forms of visible damage, but since the Sloss is below the -0.1 threshold, bulking will be minimal and the perimeter drive will remain serviceable for the entire PC2-3 LoM.

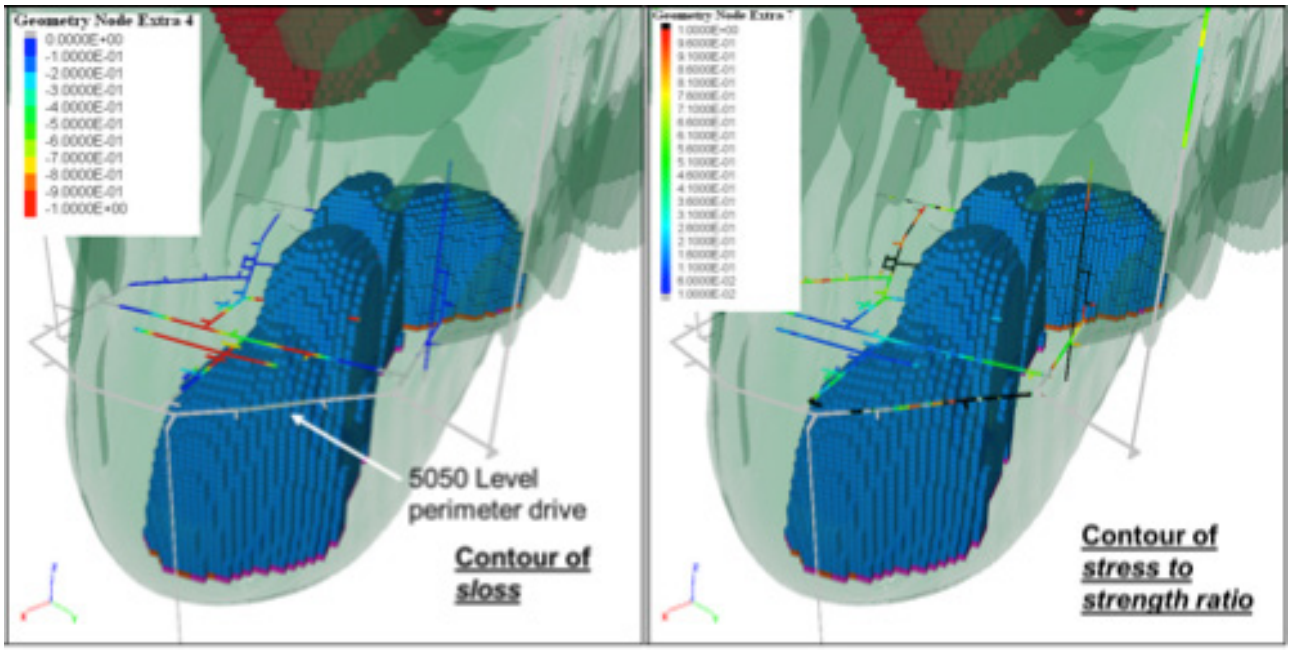

Figure 18 Sloss (left) and stress to strength ratio (right) painted over the underground infrastructure wireframe at FY35

5 Conclusions

A model was calibrated for the Cadia East mine based on the observed fracture limits for FY17, FY18, and FY19 during production from PC1 and PC2. The caving model benefitted from Itasca's strain-softening constitutive model (IMASS) that uses two-stage softening behavior. This combined with implementation of pre- and post-conditioning of the rock mass (hydraulic fracturing program) in the simulation by using

ubiquitous joints and a buckling scheme was successful in capturing the cave propagation and fracture limits that were in good agreement with the observed limits.

The calibrated model was then used to forecast the evolution of the fracture limit and damage categories on the surface over the planned PC2-3 LoM. It predicts that caving would not affect the serviceability of the public infrastructure on the surface. Similarly, no interaction was observed between the cave and the Cadia Hill open pit at the end of production. It was recommended to map the surface cracks as the cave progresses to establish a better correlation between the predicted surface damage categories from the model and observed surface cracking. This would help gain a more accurate anticipation of damage to the surface infrastructure when category four damage intersects them.

The serviceability limit for critical vent raises was assessed by using damage proxies in the model that mainly correlate to bulking of the rock mass. The model predicts that the existing and planned drives will be serviceable for their designed lifetime. Most critical vent raises are also shown to be serviceable until the end of production of PC2-3.

Acknowledgements

The authors acknowledge the support of Newcrest Mining Limited for allowing the publication of this paper, and the Cadia East Geotechnical team for providing insights into the mine's ground behavior.

References

Barton, N & Kjaernsli, B 1981, 'Shear strength of rockfill', Journal of Geotechnical and Geoenvironmental Engineering, 107(ASCE 16374).

Board, M & Pierce, M 2009, 'A review of recent experience in modelling of caving, International Workshop on Numerical Modelling for Underground Mine Excavation Design', June 28 2009, Asheville, in conjunction with the 43rd US Rock Mechanics Symposium.

Bouzeran, L, Pierce, M, Andrieux, P & Williams, E 2019, 'Accounting for rock mass heterogeneity and buckling mechanisms in the study of excavation performance in foliated ground at Westwood Mine', In Proceedings of 9th International Conference on Deep and High Stress Mining, Johannesburg, South Africa, June 2019), Australian Centre for Geomechanics.

Cavieres, P, Gaete, S, Lorig, L & Gómez, P 2003, 'Three-Dimensional Analysis of Fracturing Limits Induced by Large Scale Underground Mining at El Teniente Mine', In Proceedings of 39th U.S. Rock Mechanics Symposium, Cambridge, Massachusetts (June 2003), pp. 893–900.

Cuello, D & Newcombe, G 2018, 'Key geotechnical knowledge and practical mine planning guidelines in deep, high-stress, hard rock conditions for block and panel cave mining,' In Proceedings of the Fourth International Symposium on Block and Sublevel Caving, Australian Centre for Geomechanics, pp. 17-36.

Flores-Gonzalez, G 2019, 'Major hazards associated with cave mining: are they manageable?', in J Wesseloo (ed.), Proceedings of the First International Conference on Mining Geomechanical Risk, Australian Centre for Geomechanics, Perth, pp. 31-46.

Harrison, P 2011, 'Mine Subsidence', Chapter 8.9 of Society of Mining Engineers Handbook, pp. 627-644.

Itasca Consulting Group, Inc. 2019, FLAC3D — Fast Lagrangian Analysis of Continua in Three Dimensions Ver. 7.0. Minneapolis: Itasca.

Lee, M 2012, Cadia East – Review of Rock Stress Measurements, AMC Consultants Pty Ltd report to Newcrest Mining Limited. AMC 111153: February 2012.

Lowther, RJ, Olivier, L, Lett, JL & Brunton, I 2016, 'Implementation of a surface-based hydraulic fracturing program to successfully propagate a large cave through hard, competent near-surface rock masses to achieve breakthrough', in C Carr & G Chitombo (eds), Proceedings of MassMin 2016, pp. 83-96.

Manca, L & Flores, G 2013, 'Modern planning practices for cave mining', In Proceedings of the Third International Seminar on Mine Planning, Gecamin, Santiago.

Newcrest 2018, 'Cadia Expansion Pre-Feasibility Study Findings, Market Release', pp. 9 [22 August 2018], Available from: https://www.newcrest.com/sites/default/files/2019-10/180822_Cadia%20Expansion%20Pre%20Feasilbility%20Study%20Findings%20-%20MR.pdf

Pappas, D & Mark, C 1993, Behavior of Simulated Longwall Gob Material, Report of Investigations, 9458 USBM.

Pardo, C & Rojas, E 2016, 'Selection of exploitation method based on the experience of hydraulic fracture techniques at El Teniente Mine', in C Carr & G Chitombo (eds), Proceedings of MassMin 2016, The Australasian Institute of Mining and Metallurgy, Melbourne.

Sainsbury, BL 2012, A Model for Cave Propagation and Subsidence Assessment in Jointed Rock Masses, PhD thesis, The University of New South Wales, Sydney.

Sainsbury, BL, Sainsbury, DP & Pierce, ME 2011, 'A historical review of the development of numerical cave propagation simulations', In Continuum and Distinct Element Numerical Modeling in Geomechanics-2011, Proc. 2nd Int. FLAC/DEM Symp., Melbourne, pp. 14-16.